IOP Publishing Superconductor Science and Technology
Supercond. Sci. Technol. **28** (2015) 095018 (8pp) doi:10.1088/0953-2048/28/9/095018

Drastic improvement of the trapped field homogeneity in a superconducting hollow bulk by the insertion of a high-J_c superconducting cylinder for NMR bulk magnets

Hiroyuki Fujishiro[1], Yoshitaka Itoh[2], Yousuke Yanagi[2] and Takashi Nakamura[3]

[1] Faculty of Engineering, Iwate University, 4-3-5 Ueda, Morioka 020-8551, Japan
[2] IMRA Material R&D Co. Ltd, 2-1 Asahi-machi, Kariya 448-0032, Japan
[3] RIKEN, 2-1 Hirosawa, Wako 351-0198, Japan

E-mail: fujishiro@iwate-u.ac.jp

Received 17 June 2015, revised 16 July 2015
Accepted for publication 24 July 2015
Published 18 August 2015

Abstract

Three-dimensional (3D) numerical simulation has been performed for the field-cooled magnetization (FCM) process of REBaCuO superconducting bulk cylinders applicable to the bulk magnet for a 200 MHz (4.7 T) nuclear magnetic resonance (NMR). The influence of the position and size of the defect in the bulk on the inhomogeneity of the trapped field in the hollow space has been investigated. The trapped field profile changes depending on the position and the size of the defect, and the inhomogeneity of the trapped field can be drastically improved by inserting a superconducting thin cylinder with a critical current density (J_{c2}) higher than that of the bulk cylinder (J_{c1}). The superconducting current flows mainly on the outermost surface of the inserted thin cylinder to compensate for the inhomogeneous trapped field caused by the defect. The insertion of the superconducting thin cylinder with a higher J_{c2} is significantly effective for the practical realization of a compact NMR bulk magnet.

Keywords: numerical simulation, superconducting bulks, NMR magnet, trapped field

(Some figures may appear in colour only in the online journal)

1. Introduction

The high performance of a nuclear magnetic resonance (NMR) spectrometer has been investigated recently and an NMR superconducting magnet with a record high field of 1020 MHz (24.0 T) has been developed [1]. In superconducting magnets used in NMR spectrometers, a simultaneous ultra-high special homogeneity and stability of the magnetic field, in addition to an increased magnetic field strength, is critical. The NMR spectrometer is usually used for the research and development of synthetic organic chemistry, as it is capable of determining molecular structure. A compact and cryogen-free NMR spectrometer with a medium resolution of 200 MHz (4.7 T)–270 MHz (6.3 T) has been also desired by many laboratories in both companies and universities. This is because a large superconducting magnet system with multi-layered superconducting coils cooled by liquid helium is necessary in order to enhance the homogeneity of the magnetic field.

The REBaCuO bulk superconductor (RE: a rear earth element and Y), which can trap a higher magnetic field over 17 T [2, 3], can form a uniform trapped field in the space of the bulk cylinder, because the superconducting persistent current can flow through the bulk using field-cooled

magnetization (FCM). In 2007, a compact and cryogen-free NMR magnet was developed for the first time using annular bulk superconductors [4]. The bulk magnet, consisting of two SmBaCuO bulks with O.D. of 36 mm and I.D. of 7 mm, was cooled by a cryocooler and energized at 3 T (128 MHz); a magnetic field homogeneity of 2400 ppm was achieved in the ϕ 1.2 mm $\times$ 5.0 mm cylindrical space with a magnetic stability lasting as long as 4 months. The first NMR spectrum of ^{1}H was also observed using this bulk magnet. In 2011, a new bulk magnet using six annular EuBaCuO bulks with O.D. of 60 mm, I.D. of 16 mm and height of 70 mm was developed for the 4.7 T (200 MHz) NMR spectrometer. The ^{1}H NMR spectra of toluene with a full width at half of the maximum (FWHM) of 0.4 ppm (80 Hz) were observed with a 10 mm diameter bore at room temperature [5]. The first magnetic resonance imaging (MRI) system was also developed using annular EuBaCuO bulks [6]. A magnetic field homogeneity of 37 ppm was achieved in a ϕ 6.2 mm $\times$ 9.1 mm cylindrical space with first order shimming, which was performed by adjusting the offset current of the three axes' gradient coils. Using the MRI system, a clear three-dimensional (3D) MR image of a chemically fixed mouse fetus was observed. Recently, a visualization technique for a precise magnetic field distribution in the bulk hole magnet, which uses an MRI-based method and would be useful for developing high-quality superconducting bulk magnets, has been proposed [7].

Using the top-seeded melt growth (TSMG) method, single-grain REBaCuO bulk superconductors can be grown, resulting in the formation of growth sector boundaries (GSBs) with a higher critical current density J_c and growth sector regions (GSRs) with a relatively lower J_c [8]. As a result, a four-fold trapped field inhomogeneity necessarily exists in the hole of the bulk ring. A superconducting bulk is a composite material, in which RE_2BaCuO_5 (RE211) non-superconducting particles and Pt and Ag particles are embedded in the matrix of *c*-axis-oriented $REBa_2Cu_3O_7$ (RE123) superconducting phase. Voids and crystal defects such as twin boundaries are also created during the crystal growth. An inhomogeneous distribution of the secondary phases results in an inhomogeneous supercurrent flow in the bulk. As a result, the trapped field inhomogeneity exists in the superconductors themselves. It is necessary to understand how the size and position of these secondary phases influence the inhomogeneity of the trapped field. We refer to these non-superconducting secondary phases as 'defects'.

A recent proposal, in which a cylinder wrapped by high-temperature superconducting (HTS) tape with a higher J_c is inserted in the bulk cylinder, was experimentally confirmed to be effective in reducing the inhomogeneity of the trapped field in the hollow space [9]. The numerical simulation technique is a valuable tool to understand these problems. However, there are no reports numerically demonstrating the problems concerning the effect of the HTS cylinder. We have constructed a numerical model for the magnetizing processes in the superconducting bulk disk during FCM and pulsed field magnetization (PFM) [10, 11].

In this paper, we performed a 3D simulation during FCM on the bulk cylinder for the application of a 200 MHz NMR spectrometer. The influence of the inhomogeneous J_c distribution caused by the defects on the trapped field profile was investigated. The drastic improvement on the homogeneity of the trapped field due to the insertion of a superconducting thin cylinder was discussed.

2. Modeling and numerical simulation

A 3D model of the REBaCuO bulk cylinder using the 200 MHz NMR bulk magnet was constructed. Figure 1 shows the framework of a half cylinder model for the numerical simulation for FCM. The REBaCuO bulk cylinder has an O.D. of 60 mm, an I.D. of 28 mm and a height of 120 mm. The magnetizing coil for FCM (O.D. of 150 mm, I.D. of 100 mm and an infinite height) was placed and a static magnetic field of $B_{ex} = 4.7$ T was applied to the bulk cylinder above the superconducting transition temperature $T_c = 90$ K. Then the bulk cylinder was cooled to $T_s = 50$ K and the static magnetic field was decreased to zero at a rate of -0.0235 T min^{-1}. The physical phenomena that occurred during FCM are described using fundamental electromagnetic equations. The details of the numerical simulation are described elsewhere [10, 11]. Briefly, the following power-*n* model ($n = 100$) was used to describe the nonlinear *E-J* characteristic of the superconducting bulk,

$$E = E_c\left(\frac{J}{J_c}\right)^n, \tag{1}$$

where J_c is the critical current density and E_c ($=10^{-4}$ V m^{-1}) is the reference electric field. The constant $J_c = J_{c1} = 4.8 \times 10^8$ Am^{-2}, which is a typical J_c in the GdBaCuO bulk at $T_s = 50$ K, was assumed for the bulk cylinder [12]. For simplicity, the J_c is independent of any applied magnetic field, such as a Bean's model, in the following [13],

$$\mathrm{rot}E = -\frac{dB}{dt} \tag{2}$$

$$\mathrm{rot}B = \mu_0 J. \tag{3}$$

According to equation (2), the electric field E is generated in the bulk in the descending process of the external magnetic field. As a result, the current J flows in the bulk according to equation (1), and the magnetic field gradient takes place according to equation (3).

Photo-Eddy commercial software (Photon Ltd, Japan) was used to analyze the electromagnetic field using the finite element method. Iterative calculations were performed to obtain the electromagnetic field in the superconductor at each time step. In the numerical analysis, the bulk cylinder was equally divided into 20 elements along the circumferential direction and 16 elements along the radial direction. Along the *z* direction, a mesh was created as shown in figure 1. In the hollow space within $x = y = \pm 5$ mm, a mesh was created with 1 mm spacing.

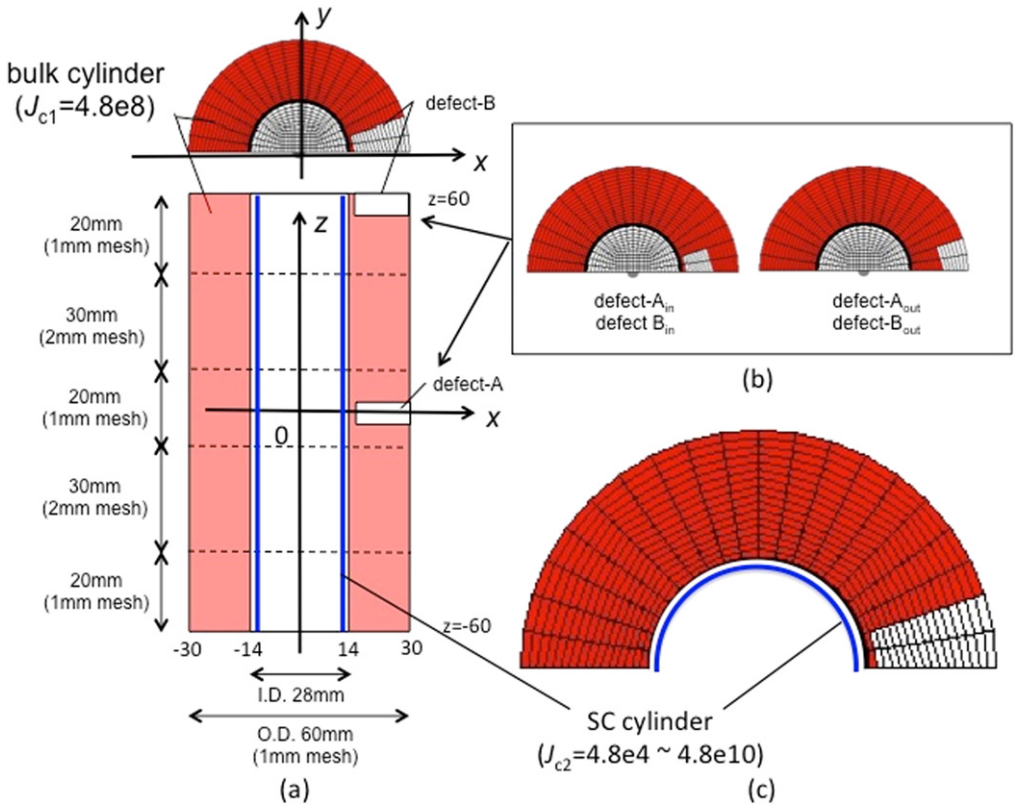

Figure 1. (a) Half model of the framework for the numerical simulation of FCM, in which the dimension of the bulk cylinder and the position of the defect-A and defect-B are shown. (b) The size and position of the 'defect-A_{in} (or defect-B_{in})' and 'defect-A_{out} (or defect-B_{out})'. (c) The superconducting (SC) thin cylinder inserted inside the bulk cylinder.

Two types of unrealistically large defects (defect-A and defect-B) with a J_c of zero were introduced in the bulk cylinder in order to emphasize the influence of the defects on the inhomogeneity of a magnetic field, in addition to a uniform bulk cylinder without any defects. The positions of both defects are shown in figure 1, where defect-A is located at the centre ($z = 0$ mm), which can be understood as the influence of the defect near the centre on the inhomogeneity of the trapped field. Defect-B is located at the top surface ($z = 60$ mm) of the bulk cylinder, which can be clarified as the influence of the defect far from the centre. The dimensions of the defects are 2 elements (18 deg.) along the circumferential direction, 15 elements (15 mm) along the radial direction and 8 elements (8 mm) in thickness. Note that the innermost element between $x = 14$ and 15 mm remains as superconducting bulk, through which a superconducting current barely flows along the circumferential direction. In order to investigate the influence of defect size and the position along the x-direction, two types of defects were also prepared for each defect; as shown in figure 1(b), 'defect-A_{in}' and 'defect-B_{in}' have 8 elements along the radial direction from $x = 15$ to 23 mm and 'defect-A_{out}' and 'defect-B_{out}' have 8 elements from $x = 23$ to 30 mm.

In order to clarify the effect of inserting another superconducting cylinder inside the bulk cylinder, a superconducting thin cylinder with an O.D. of 27 mm, I.D. of 26 mm and height of 120 mm was inserted in the hollow bulk, as shown in figure 1(c). The J_c value of the superconducting thin cylinder was changed from $J_c = J_{c2} = 4.8 \times 10^4$ to 4.8×10^{10} Am^{-2}. The improvement to the magnetic field profile in the hollow space was investigated along the x- and z-directions.

3. Results of numerical simulation

3.1. Influence of the position and size of a defect on the inhomogeneity of the trapped field

Figures 2(a) and (b) present the cross-sections of the macroscopic trapped field profile along the x-direction at $y = z = 0$ and along the z-direction at $x = y = 0$ for the uniform, defect-A and defect-B bulks, respectively. In figure 2(a), along the x-direction, a trapezoidal B_z profile can be obtained for each bulk, which suggests that the applied field of 4.7 T to the bulk cylinder with $J_{c1} = 4.8 \times 10^8$ Am^{-2} is insufficient for full magnetization. For the defect-A bulk, the chipping in the B_z profile along the $+x$-direction can be seen asymmetrically at $x = +15$ mm in the vicinity of the defect-A. On the other hand, the B_z-x profile for the defect-B bulk shows a similar symmetric profile to that of the uniform bulk because the position is far from the defect-B. In figure 2(b) along the z-direction, the symmetric B_z-z profile can be obtained for defect-A as well as for the uniform bulks. However, a steep B_z decrease can be seen at $z > +30$ mm in the defect-B bulk, as the defect-B affects the trapped field profile near the defect.

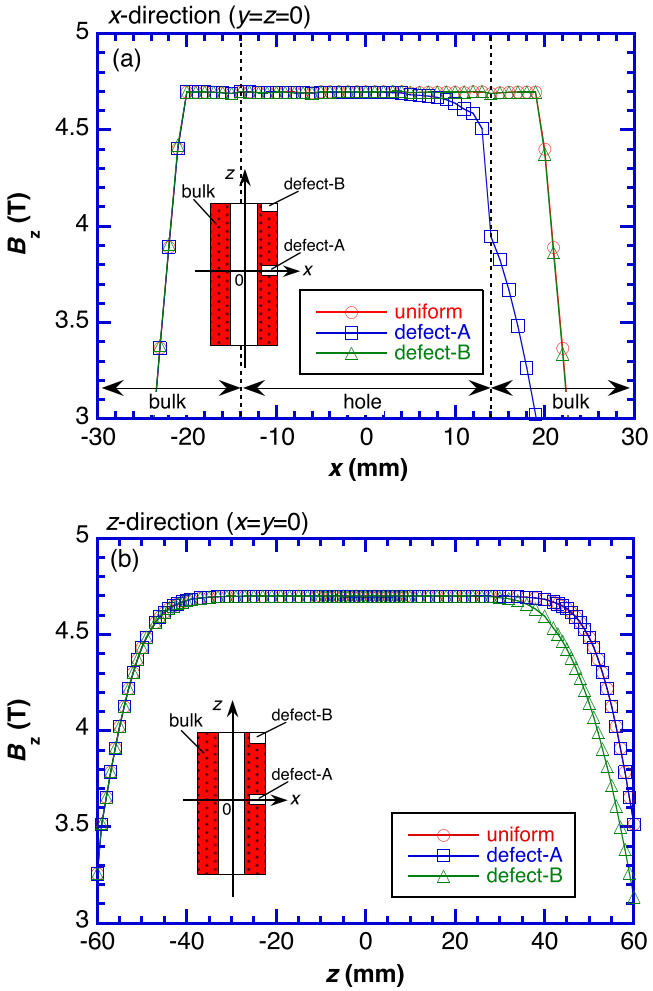

Figure 2. The cross-sections of the macroscopic trapped field profile for the uniform, defect-A and defect-B bulks (a) along the x-direction at $y = z = 0$ and (b) along the z-direction at $x = y = 0$.

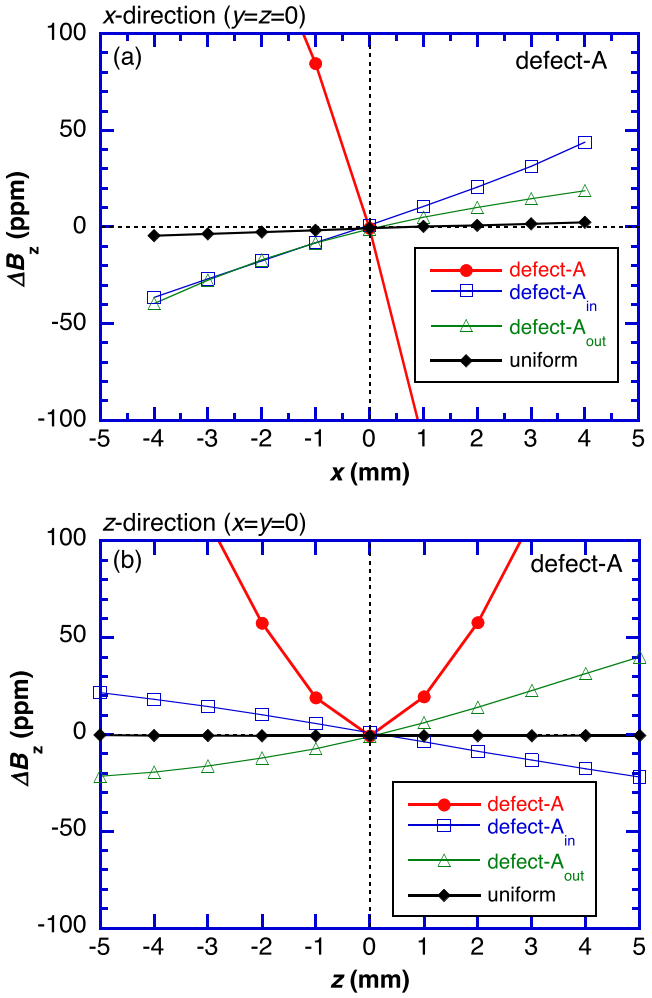

Figure 3. Trapped field deviation ΔB_z around the central region (a) along the x-direction ($-4 \leqslant x \leqslant 4$ mm) at $y = z = 0$ and (b) along the z-direction ($-5 \leqslant z \leqslant 5$ mm) at $x = y = 0$ in the bulk-hole for the defect-A bulk and uniform bulk. The results of the defect-A_{in} and defect-A_{out} bulks are also shown.

Figures 3(a) and (b) show the microscopic trapped field deviation ΔB_z around the central region along the x-direction ($-4 \leqslant x \leqslant 4$ mm) at $y = z = 0$ and along the z-direction ($-5 \leqslant z \leqslant 5$ mm) at $x = y = 0$ in the hollows of the uniform and defect-A bulks, respectively. ΔB_z is defined by $(B_z\text{-}B_z(0))/B_z(0)$, where $B_z(0)$ shows the B_z value at the centre of the hollow ($x = y = z = 0$). The ΔB_z of the defect-A bulk was very large along both the x- and z-directions. Although the ΔB_z for the uniform bulk should be zero in principle, the obtained ΔB_z was within 5 ppm along the x- and z-directions due to the errors derived from significant digits in the EFM calculation.

The trapped field deviation ΔB_z of the defect-A_{in} and defect-A_{out} bulks is also shown in figure 3. It was found that the ΔB_z values of the defect-A_{in} and defect-A_{out} became smaller due to the decrease of the defect size. The defect-A_{out}, located farther from the center has a smaller ΔB_z value than that of defect-A_{in}. The relationship between the size and position of the defect and the inhomogeneity of the trapped field profile cannot be easily explained, since it is a product of the integration of the 3D current distribution. However, qualitatively speaking, the current distribution becomes inhomogeneous around the defects, where a current density nearly identical to J_{c1} might flow, even on the inner side of the bulk cylinder.

Figures 4(a) and (b), respectively, depict the microscopic trapped field deviation ΔB_z around the central region along the x-direction ($-4 \leqslant x \leqslant 4$ mm) at $y = z = 0$ and along the z-direction ($-5 \leqslant z \leqslant 5$ mm) at $x = y = 0$ in the hole of the uniform and defect-B bulks. The results for the uniform bulk were also reused. The ΔB_z for the defect-B bulk was small along the z-direction, while the gradient of the B_z-x relation was the opposite. This is in clear contrast with those for the defect-A. The deviation ΔB_z of the defect-B_{in} and defect-B_{out} bulks is also shown in figure 4. Similarly to the cases in defect-A_{in} and defect-A_{out}, the ΔB_z was influenced by the size and the position of defect-B. However, the influence of the position is slightly different in the case of defect-A, as shown in figure 3.

3.2. Improvement effect of inserting the superconducting cylinder on trapped field uniformity

In order to apply the superconducting bulks to the NMR spectrometer, it is necessary to enhance the uniformity of the trapped field in the hollow of the bulk cylinder to as high an

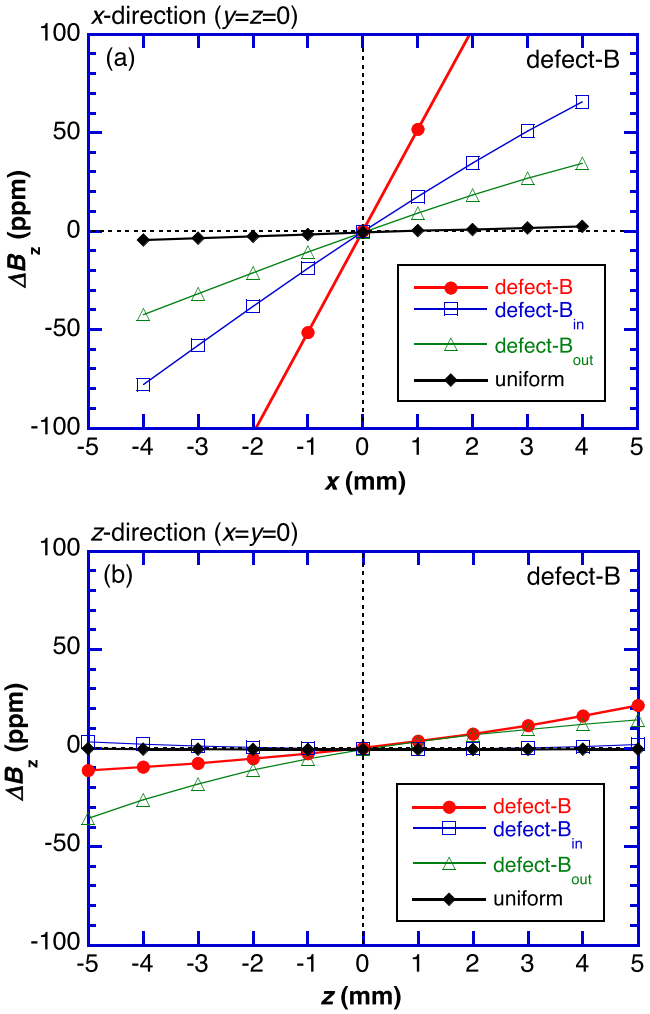

Figure 4. The microscopic trapped field deviation ΔB_z around the central region (a) along the x-direction ($-4 \leqslant x \leqslant 4$ mm) at $y = z = 0$ and (b) along the z-direction ($-5 \leqslant z \leqslant 5$ mm) at $x = y = 0$ in the hole of the defect-B bulk and uniform bulk. The results of the defect-B_{in} and defect-B_{out} bulks are also shown.

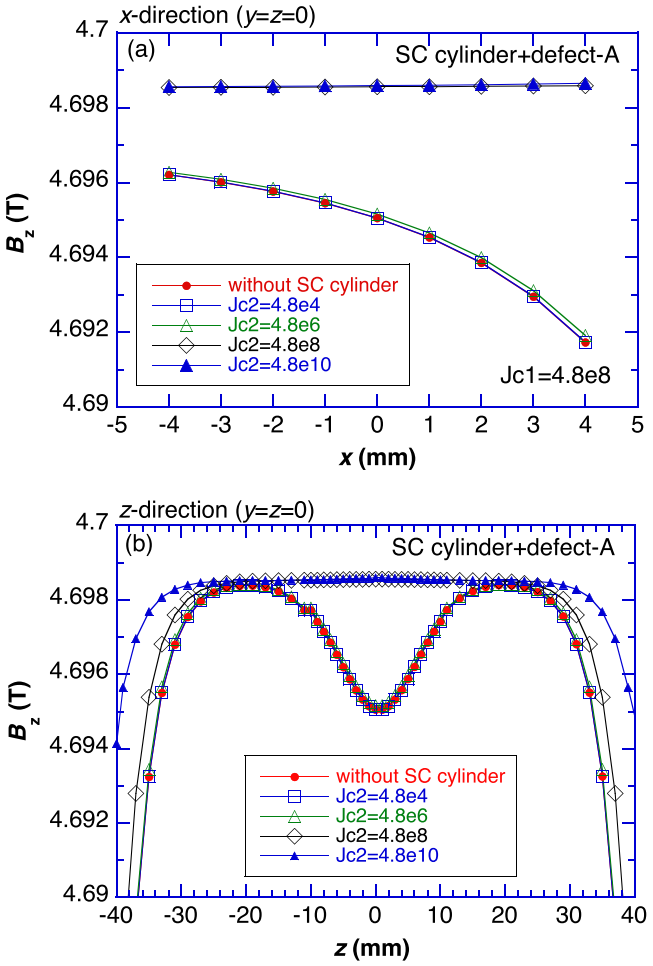

Figure 5. The trapped field profile along the x-direction and the z-direction in the defect-A bulk with a superconducting cylinder insert, as a function of the critical current density J_{c2} of the inserted superconducting cylinder.

extent as possible. Our group clarified that inserting a cylinder wrapped in high-temperature superconducting (HTS) tape is an experimentally effective method to reduce the inhomogeneity of the trapped field [9]. In this subsection, the cylinder wrapped in HTS tape is replaced by the ideal superconducting thin cylinder with a higher critical current density J_{c2}, and the relationship between the J_{c2} of the inserted cylinder and the uniformity of the trapped field was investigated using numerical simulation.

Figures 5(a) and (b) present the macroscopic trapped field profile along the x- and z-directions in the defect-A bulk with the superconducting cylinder insert, respectively, as a function of J_{c2} of the inserted superconducting cylinder. In this case, the J_c of the bulk cylinder is $J_c = J_{c1} = 4.8 \times 10^8\,\mathrm{Am}^{-2}$. For J_c, from 4.8×10^4 to $4.8 \times 10^6\,\mathrm{Am}^{-2}$, no effect can be seen from the insertion of the superconducting cylinder. For $J_{c2} = 4.8 \times 10^8\,\mathrm{Am}^{-2}$, which is the same as that of the bulk cylinder, the magnetic profile along the x-direction became drastically flat. At the same time, the profile along the z-direction also became drastically flat, becoming slightly wider toward the outside region. For $J_{c2} = 4.8 \times 10^{10}\,\mathrm{Am}^{-2}$, which is two orders of magnitude larger than the J_{c1} of the bulk cylinder, the profile along the x-direction still remained, with the flat profile along the z-direction widening toward the outer region as well. In this way, the homogeneity of the magnetic field in the hollow cylinder can be drastically recovered by inserting a superconducting cylinder with a higher J_{c2} than that of the bulk cylinder with J_{c1}.

Figures 6(a) and (b) show the trapped field profiles along the x- and z-directions, respectively, in the defect-B bulk with the superconducting cylinder insert as a function of J_{c2} of the superconducting cylinder. For a J_{c2} from 4.8×10^4 to $4.8 \times 10^6\,\mathrm{Am}^{-2}$, the cylinder insertion had no influence on the trapped field profile. For $J_{c2} = 4.8 \times 10^8\,\mathrm{Am}^{-2}$, the same as J_{c1} of the bulk, the inhomogeneity of the trapped field along the x-direction was suppressed slightly and the flatness of the trapped field also widened along the z-direction. For $J_{c2} = 4.8 \times 10^{10}\,\mathrm{Am}^{-2}$, two orders of magnitude larger than J_{c1} of the bulk, the trapped field along the x-direction and z-direction became flat. It should be noted that the effect of inserting the superconducting thin cylinder with

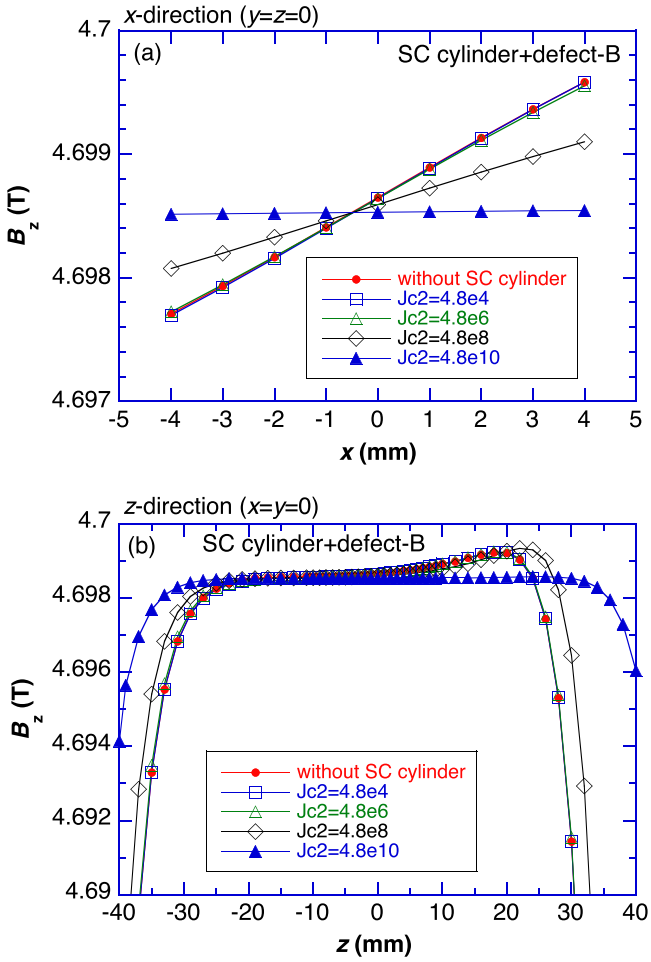

Figure 6. The trapped field profile along the x-direction and the z-direction in the defect-B bulk with a superconducting cylinder insert, as a function of the J_{c2} of the inserted superconducting cylinder.

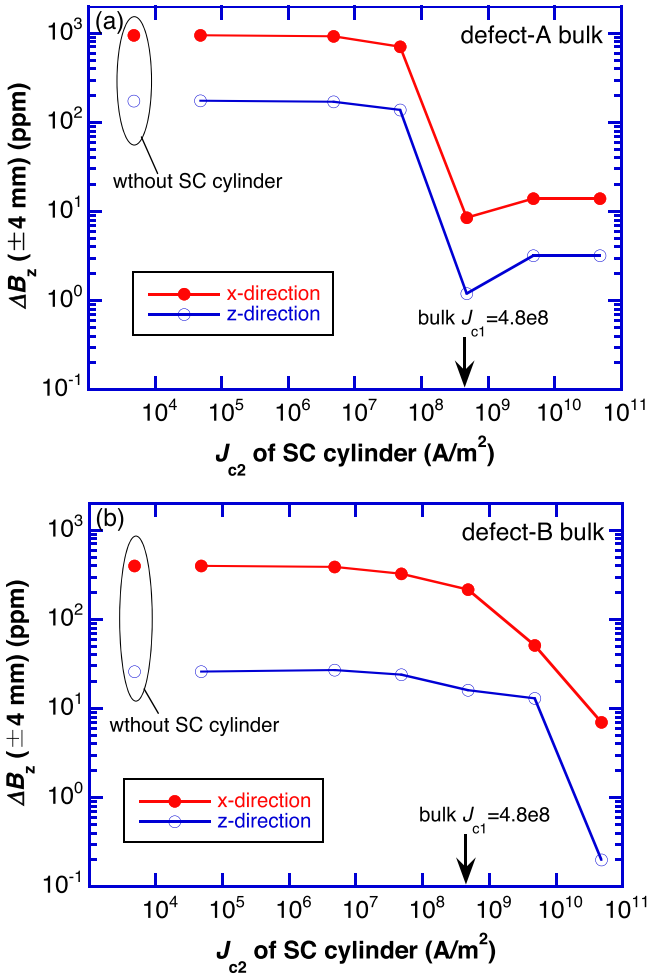

Figure 7. The trapped field deviation $\Delta B_z(\pm 4\,\mathrm{mm})$ along the x-direction ($-4 \leqslant x \leqslant 4$ mm) at $y = z = 0$ and along the z-direction ($-4 \leqslant z \leqslant 4$ mm) at $x = y = 0$ in the hole for (a) defect-A and (b) defect-B bulks, as a function of the J_{c2} of the inserted superconducting cylinder.

$J_{c2} = 4.8 \times 10^8\,\mathrm{Am}^{-2}$ on the defect-B bulk was slightly different from that on the defect-A bulk, shown in figure 5. This is due to the differences between the distributions of the superconducting current depending on the position of the defect. In this way, the homogeneity of the magnetic field caused by defect-B in the hollow cylinder can be recovered by the insertion of a superconducting cylinder with J_{c2} higher than that of the bulk cylinder with J_{c1}.

Figures 7(a) and (b) summarize the trapped field deviation $\Delta B_z(\pm 4\,\mathrm{mm})$ along the x-direction ($-4 \leqslant x \leqslant 4$ mm) at $y = z = 0$ and along the z-direction ($-4 \leqslant z \leqslant 4$ mm) at $x = y = 0$ in the hole of the defect-A and defect-B bulks, respectively, as a function of the J_{c2} of the inserted superconducting cylinder. In the defect-A bulk, the improvement effect of the trapped field profile can clearly be obtained with a J_{c2} value of the inserted superconducting cylinder higher than $4.8 \times 10^8\,\mathrm{Am}^{-2}$ in both the x- and z-directions. The ΔB_z minimum at $J_{c2} = 4.8 \times 10^8\,\mathrm{Am}^{-2}$ is not an essential character, and may come from an error in the FEM calculation. On the other hand, for the defect-B bulk, the improvement effect can clearly be obtained with a J_{c2} value higher than $4.8 \times 10^{10}\,\mathrm{Am}^{-2}$. The difference may come from the relationship between the configuration of the defect and the J_{c2} value of the superconducting thin cylinder.

4. Discussion

In order to understand the reason why the insertion of the superconducting cylinder with higher J_{c2} improved the trapped field profile in the hollow space of the bulk cylinder, we analyzed the superconducting current distribution in the superconducting thin cylinder. Figures 8(a) and (b) show the calculated superconducting current distributions in the outermost surface of the thin cylinder with $J_{c2} = 4.8 \times 10^{10}\,\mathrm{Am}^{-2}$ inserted in the defect-A and defect-B bulks, respectively. Schematic views of the current distributions are also shown in figures 8(c) and (d) for each bulk. For both bulks, the circular current J with nearly the same value as J_{c2} flows into both ends of the thin cylinder to compensate for the decrease of the trapped field at the bulk edges. In addition, for the defect-B bulk, the additional circular current also flows at the edge of the thin cylinder facing defect-B in

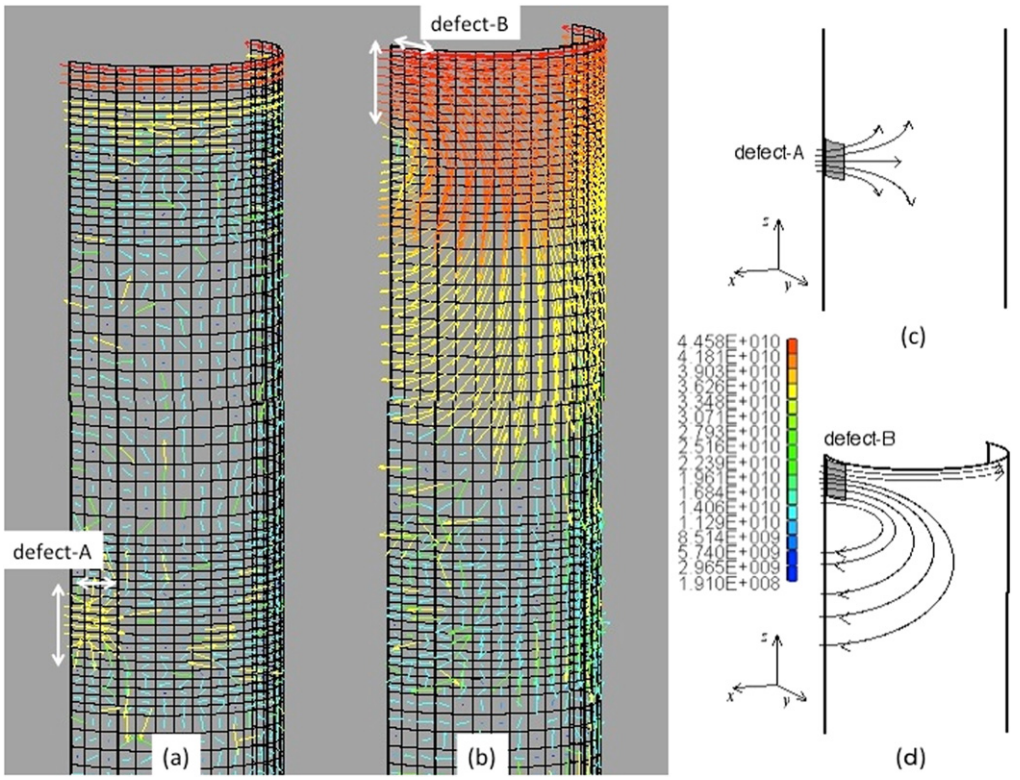

Figure 8. The results of the simulation of the superconducting current distribution in the outermost surface of the thin cylinder for (a) the defect-A bulk and (b) the defect-B bulk, in which the J_{c2} is 4.8×10^{10} Am^{-2}. Schematic views of the superconducting current distribution are also shown in (c) and (d) for each bulk.

order to compensate for the decrease of the trapped field caused by defect-B. On the other hand, for the defect-A bulk, the superconducting circular current flows in the thin cylinder facing defect-A, which is smaller than that of the thin cylinder facing defect-B, to compensate for the decrease in the trapped field due to defect-A. For the innermost surface as well as the inside of the thin cylinder, no remarkably large supercurrent was found to flow. A large superconducting current to compensate for the decrease in the magnetic field due to the defects mainly flows in the outermost surface of the thin cylinder with a higher J_{c2}. The J_c values in REBaCuO-coated conductors have been enhanced over 10^{10} Am^{-2} under the magnetic field of several tesla at 50 K [14, 15]. The J_{c2} value as large as 10^{10} Am^{-2} can be practically attainable at present. In this way, the mechanism, in which the homogeneity of the trapped field can be improved via the insertion of a superconducting thin cylinder, can be explained qualitatively by the rearrangement of the superconducting current within the thin cylinder.

Finally, we discuss the difference between the realistic bulk superconductor and the bulk model in the simulation. In the present analysis, unrealistically large defects are intentionally introduced in the hollow bulk superconductor in order to enhance the effect of inserting the superconducting cylinder on the trapped field distribution. In the realistic bulk superconductors, the defects are much smaller, and more or less uniformly distributed throughout the bulk. This study is the first step towards understanding the relationship between the size and position of the defect and the trapped field uniformity. We want to apply this technique to the realistic model for the bulk superconductors.

5. Summary

A three-dimensional (3D) numerical simulation has been performed for the field-cooled magnetization (FCM) process of REBaCuO superconducting bulk cylinders applicable to a 200 MHz NMR (4.7 T) bulk magnet. The influence of the position and size of the defect ($J_c = 0$) in the bulk on the homogeneity of the trapped field in the hollow space has been investigated. The important results and conclusions obtained from this study are summarized as follows.

(1) The trapped field profile changes depending on the position and size of the defect, as evidenced by the cases of defect-A, situated near the centre, and defect-B, situated in the bulk edge. The trapped field deviation ΔB_z at the central region, which is defined by $(B_z\text{-}B_z(0))/B_z(0)$, along the x- and z-directions decreased with the decreasing size of the defect in both cases. The defect situated inside the bulk cylinder had a moderate influence on the inhomogeneity of the trapped field distribution in the hollow space.

(2) The inhomogeneity of a trapped field due to defects can be improved drastically via the insertion of a superconducting thin cylinder with a higher critical current density than that

of the bulk cylinder. The insertion effect creates a slight difference along the x- and z-directions for both defect bulks, which may be caused by the relationship between the configuration of the defect and the superconducting current distribution flowing in the thin cylinder.

(3) In the case of defect-B bulk, when inserting the superconducting thin cylinder with a J_{c2} of two orders of magnitude higher than that of the bulk cylinder J_{c1}, it was found that a large circular current flows in the thin cylinder facing defect-B to compensate for the decrease in the trapped field caused by defect-B, in addition to the circular current with nearly the same value as J_{c2} at both ends of the cylinder. For the defect-A bulk, only a relatively smaller superconducting current flows in the thin cylinder facing defect-A. Only the superconducting current flowing in the outermost surface of the thin cylinder is effective at compensating for the inhomogeneity of the trapped field. The mechanism with which to improve the inhomogeneity of the trapped field can be explained qualitatively by rearranging the superconducting current in the thin cylinder.

Acknowledgements

The authors thank Dr T Naito of Iwate University for the valuable discussion. This study was financially supported by the 'Development of System and Technology for Advanced Measurement and Analysis' project of the Japan Science and Technology Agency (JST).

References

[1] Ohki S *et al* 2015 *J. Magn. Reson.* **256** 30–3
[2] Tomita M and Murakami M 2003 *Nature* **421** 517–20
[3] Durrell J H *et al* 2014 *Supercond. Sci. Technol.* **27** 082001
[4] Nakamura T, Itoh Y, Yoshikawa M, Oka T and Uzawa J 2007 *Concepts Magn. Reson.* B **31B** 65
[5] Nakamura T, Itoh Y, Yoshikawa M, Sakai N, Nariki S, Hirabayashi I and Utsumi H 2011 *J. Cryo. Soc. Japan* **46** 139–48 (in Japanese)
[6] Ogawa K, Nakamura T, Terada Y, Kose K and Haishi T 2011 *Appl. Phys. Lett.* **98** 234101
[7] Tamada D, Nakamura T, Itoh Y and Kose K 2013 *Physica* C **492** 174–7
[8] Sakai N *et al* 2011 *J. Cryo. Soc. Japan* **46** 131–8 (in Japanese)
[9] ltoh Y, Yanagi Y and Yoshikawa M 2014, *Japanese Patent Application No*. 2014-127301
[10] Fujishiro H and Naito T 2010 *Supercond. Sci. Technol.* **23** 105021
[11] Fujishiro H, Naito T and Yoshida T 2014 *Supercond. Sci. Technol.* **27** 065019
[12] Kii T *et al* 2012 *IEEE Trans. Appl. Supercond.* **22** 4100904
[13] Bean C P 1962 *Phys. Rev. Lett.* **8** 250
[14] Inoue M *et al* 2013 *IEEE Trans. Appl. Supercond.* **23** 8002304
[15] Awaji S and Watanabe K 2011 *Supercond. Cryo.* **13** 1